RSC Advances

PAPER

Cite this: *RSC Adv.*, 2014, **4**, 59275

Ultrasensitive detection and co-stability of mercury(II) ions based on amalgam formation with Tween 20-stabilized silver nanoparticles†

Zhi Guo,[ab] Guiqiu Chen,*[ab] Guangming Zeng,*[ab] Zhongwu Li,[ab] Anwei Chen,[c] Ming Yan,[ab] Lingzhi Liu[ab] and Daoyou Huang[d]

Received 25th July 2014
Accepted 29th October 2014

DOI: 10.1039/c4ra07621d

www.rsc.org/advances

A rapid and sensitive colorimetric sensing strategy employing silver nanoparticles (AgNPs) to detect trace Hg^{2+} in aqueous solutions is described. The citrate-capped AgNPs were functionalized to form a Tween 20-stabilized AgNPs (Tween 20-AgNPs) probe, which was stable in a high ionic strength environment. When Hg^{2+} was present in the aqueous solution, citrate reduced Hg^{2+} to Hg^{0} and formed a Ag/Hg amalgam with the AgNPs, followed by the removal of Tween 20 from the surface of the AgNPs. The AgNPs were unstable in high ionic strength solutions, resulting in AgNPs aggregation and co-stabilization with Hg^{2+}, observed by a decrease in the UV-vis absorption. This decrease in the UV-vis absorption was proportional to the concentration of Hg^{2+}. Under optimized conditions, the sensing system exhibited a linear range of 5.0×10^{-10} to 1.2×10^{-7} M for Hg^{2+}, with a detection limit of 0.31 nM in buffer. The co-stabilization assays showed no Hg^{2+} was detected to be remaining in solution using our proposed method. The AgNPs removal percentage was correlated well with the concentration of Hg^{2+} with a correlation coefficient of 0.99862. When the concentration of Hg^{2+} was in excess, the AgNPs removal percentage correlated with the concentration of AgNPs with a correlation coefficient 0.994 as well. Moreover, this probe was successfully used to detect and co-stabilize Hg^{2+} in tap water, spring water, and surface water samples.

1. Introduction

Heavy metal pollution has been an important concern throughout the world for decades because of the severe risks posed by heavy metals to human health and the environment. Among them, Hg^{2+} is the among the most noted ions due to the damage it causes to the brain, nervous system, and endocrine system.[1,2] And Ag^{+}, most probably released from AgNPs, is widely distributed in our surroundings.[3,4] These two heavy metal ions exhibit serious adverse effects on the human body and other biology in toxicology studies.[5–7] Therefore, it is important to develop efficient methods for the selective and sensitive detection of trace Hg^{2+}. The development of novel methods to stabilize metals is urgently needed to protect our environment and health.

To the best of our knowledge, traditional methods for Hg^{2+} quantification (such as cold vapor atomic absorption spectrometry,[8,9] inductively coupled plasma mass spectrometry (ICP-MS),[10,11] surface-enhanced Raman scattering,[12,13] electrochemical sensing,[14,15] and stripping voltammetry,[16,17] *etc.*) always have high sensitivity and selectivity but require bulky instrumentation and extensive sample pretreatment processes that limit their application to *in situ* analysis. To overcome these limitations, researchers have developed various fluorescent and colorimetric Hg^{2+} sensing systems for the wide application of

[a]*College of Environmental Science and Engineering, Hunan University, Changsha 410082, P.R. China. E-mail: gqchen@hnu.edu.cn; zgming@hnu.edu.cn; Fax: +86 731 88823701; Tel: +86 731 88822829*

[b]*Key Laboratory of Environmental Biology and Pollution Control (Hunan University), Ministry of Education, Changsha 410082, P.R. China*

[c]*College of Resources and Environment, Hunan Agricultural University, Changsha 410128, P.R. China*

[d]*Key Laboratory for Agro-ecological Processes in Subtropical Region, Institution of Subtropical Agriculture, Chinese Academy of Science, Changsha 410125, P.R. China*

† Electronic supplementary information (ESI) available: Experimental details of the preparation of bare AgNPs and TEM images of the citrate-capped AgNPs, bare AgNPs, Tween 20-AgNPs, and Ag/Hg amalgam in the presence of 100 nM Hg^{2+} (Fig. S1). Size distribution of bare AgNPs (Fig. S2). Zeta potential measurement of the Tween 20-AgNPs (Fig. S3). Demonstration of the displacement of Tween 20 with Hg^{2+} (Fig. S4). Extinction spectra of solutions with and without the addition of 200 nM Hg^{2+} (Fig. S5). Reduction of Hg^{2+} at room temperature by using citrate in the absence of Tween 20 AgNPs (Fig. S6). EDX spectroscopy analysis of Tween 20-AgNPs and Ag/Hg amalgam (Fig. S7, Table S1 and S2). XRD analysis of Ag/Hg amalgam in the presence of 50.0 and 500.0 nM Hg^{2+} (Fig. S8). Photographs of working solutions containing Tween 20-AgNPs after adding 100 and 200 nM Hg^{2+} (Fig. S9). The calibration curve of UV-vis absorbance intensity against Hg^{2+} concentration in buffer samples and response linearity of the assay with Hg^{2+} concentrations of 0.5, 5.0, 20.0, 50.0, 80.0, 100.0, 120.0 and 200.0 nM (Fig. S10). The comparison of assay methods for monitoring mercury in linear range and MDC (Table S3), and determination of Hg^{2+} in water samples using the proposed method and AFS (Table S4). Photographs of working solutions containing Tween 20-AgNPs after adding various concentrations of Hg^{2+} in buffer (Fig. S11). See DOI: 10.1039/c4ra07621d

fluorescence and colorimetric-analysis in heavy metal ion recognition.[18–20] These systems include molecular probes using small organic molecules,[21–28] porphyrin derivative,[29,30] DNAzymes,[31–34] proteins,[35,36] and nanomaterials using nanoparticles,[37,38] nanoclusters,[39] and semiconductor quantum dots.[40–42] Although significant contributions have been made to the detection of Hg^{2+}, these approaches have low sensitivity and poor selectivity because they are based on interactions between functional groups.

More recently, a method was developed to detect trace Hg^{2+} and Ag^{+} that used Tween 20-modified gold nanoparticles as the probe.[38] This probe can react with Ag^{+}, which might interfere with the detection of Hg^{2+} in the presence of Ag^{+}. Therefore, it is desirable to develop a more suitable detection method. We found that Tween 20-modified Ag nanoparticles are a good choice for obtaining a high selectivity for Hg^{2+} and are able to form a co-stable Ag/Hg amalgam with Hg^{0}.

It is well-known that elemental mercury can form complexes with certain metals to form amalgams.[43–45] It has previously been demonstrated that Hg^{2+} can selectively integrate into DNA-protected AgNPs to form stable Ag/Hg amalgams,[46] where the dye-labeled ssDNA acted as the signal reporter. Hg^{2+} detection was achieved by forming a Ag/Hg amalgam upon reduction of the mercury species to elemental mercury, with the silver atoms acting as acceptors for the elemental mercury. The Ag/Hg amalgam is stable and easily removed from the environment. Considering these issues, a label-free, rapid, and homogeneous method for sensing Hg^{2+} using a Tween 20-stabilized AgNPs (Tween 20-AgNPs) probe was proposed. The citrate ions on the Tween 20-AgNPs surfaces reduced Hg^{2+} to elemental mercury, resulting in the formation of a Ag/Hg amalgam. This proposed method exhibits higher sensitivity than some probes previously reported and also has high selectivity toward Hg^{2+}, even in the presence of other competitive heavy metal ions. The strong selectivity toward Hg^{2+}, combined with the high stability of the Ag/Hg amalgam, provides a new and simple method for Hg^{2+} detection and Hg^{2+}/Ag^{+} stability in environmental or biological samples.

2. Experimental section

2.1. Chemicals and apparatus

All of the chemical components were of analytical grade. Tween 20 was purchased from Solarbio (Beijing, China). $AgNO_3$ (99.99%), $Hg(NO_3)_2$ (99.99%), and $NaBH_4$ (99.99%) were purchased from Sigma Aldrich. Nickel acetate (99.9%) and aluminium chloride (99.99%) were purchased from Alfa Aesar. All other metal ion stock solutions were prepared from nitrate or sulfate salts. Double distilled water was used throughout the experiments. The concentrations of the AgNPs stock solutions were analyzed with atomic absorption spectroscopy (AAS) according to a previously published protocol.[47]

UV-vis absorption was measured on a UV-visible spectrophotometer (Model UV-2550, Shimadzu, Japan). TEM measurement was made using a JEOL JEM-3010 transmission electron microscope (Beijing, China) with an accelerating voltage of 200 kV. The sample for TEM characterization was prepared by placing a drop of the sample solution on a carbon-coated copper grid and allowing it to dry at room temperature. Energy-dispersive X-ray (EDX) spectra were obtained using the TEM microscope (JEOL JEM-2100F). The XRD pattern was recorded using an automatic X-ray diffractometer (D8-Advance, Bruker Company, Germany). Hydrodynamic diameters and zeta (ζ) potentials were quantified by dynamic light scattering (DLS) conducted with a Malvern Zetasizer (Nano-ZS, Malvern Instruments, UK). AAS data were obtained from an atomic absorption spectrophotometer (AA700, Perkin-Elmer, USA). Atomic fluorescence measurements were performed on an atomic fluorescence spectrometer (AFS-9700, Beijing, China).

2.2. Synthesis of citrate-capped AgNPs

The colloidal solution of AgNPs was synthesized according to the method described by Liu *et al.*[48] with little modification. A 59.8 mL solution containing 0.6 mM trisodium citrate and 0.4 mM $NaBH_4$ was prepared in double distilled water and stirred vigorously in an ice bath. The solution turned yellow upon the addition of 0.55 mL 23.5 mM $AgNO_3$, indicating the formation of the AgNPs. After 3 h of additional stirring at room temperature, the soluble byproducts were removed by centrifugal ultrafiltration (molecular weight cutoff of 8000), and the AgNPs were washed with double distilled water. TEM images confirmed that the sizes of the AgNPs were 5.0–10.0 nm (Fig. S1A†).

2.3. Preparation of Tween 20-AgNPs

Tween 20-AgNPs were prepared using a previously published method with slight modifications.[49] Tween 20 (10% v/v, 200 μL) was added to a solution of citrate-capped AgNPs (15.204 μg mL^{-1}, 57.35 mL) with stirring. After a subsequent 0.5 h of stirring, the AgNPs were filtered and stored at 4 °C for further use. Details about the preparation of bare AgNPs (12.839 μg mL^{-1}, 12.0 ± 2 nm, Fig. S1B and S2) are described in the ESI.†

2.4. Detection of Hg^{2+}

Tween 20-AgNPs were prepared in 100 mM sodium phosphate solution. For Hg^{2+} detection, 3 mL of the as-prepared Tween 20-AgNPs mixture was added to a 10 mL volumetric pipe containing 15 μL 1.0 M sodium phosphate buffer sample. Then 35 μL $Hg(NO_3)_2$ solution of various concentrations was added. Finally, the time-gated absorbance of different concentrations of Hg^{2+} was monitored after the completion of the aggregation and stabilization. For optimizing the reaction time, 100 nM Hg^{2+} was selected as the model to evaluate the optimum reaction time. All the samples were incubated at room temperature with gentle shaking. The spring water and surface water were sampled from Yuelu Mountain and Taozi Lake in Changsha City. The absorbance was recorded at the maximum absorption peak at 400 nm.

2.5. Procedures for co-stability assays

For the co-stability assays, different concentrations of Hg^{2+} and AgNPs were mixed. Then the mixture was left for 5 h to complete

precipitation before filtration with a 0.22 μm filter membrane. The Hg^{2+} concentration in the filtration was determined by the proposed method herein and the AgNPs concentration was quantified with AAS.

The concentration of the AgNPs was determined by nitric acid/hydrogen peroxide digestion (2 mL HNO_3, 1 mL H_2O_2). AgNPs solutions (120 μL) were digested in 20 mL disposable scintillation vials for 24 h in triplicate, followed by filtration through 0.22 μm filter to get rid of impurities. The resulting filtrate volume was brought to 10 mL with 1% nitric acid (100 fold dilution) and its concentration was then determined by AAS.

3. Results and discussion

3.1. Sensing and co-stabilization mechanism

In this study, we fabricated a special probe (Tween 20-AgNPs) using Tween 20 as the stabilizer to block aggregation of citrate-capped AgNPs in high ionic strength solutions. The citrate ions on the surface of Tween 20-AgNPs act as a reducer of Hg^{2+}. The neutral Tween 20 coating acts as a shield for the citrate ions but does not displace them, which was demonstrated by the zeta potential of Tween 20-AgNPs (−14.6 mV, Fig. S3†).[38]

Fig. 1 shows the fundamental mechanism of Tween 20-AgNPs sensing and co-stabilization of Hg^{2+}. We reasoned that the citrate ions capping the AgNPs surface can act as a reducing agent for Hg^{2+} when the citrate-capped AgNPs had been modified with Tween 20.[50] When Hg^{2+} was present, silver atoms acted as the acceptors for elemental mercury. The reduced elemental mercury was directly deposited onto the Ag surface due to the high affinity between Ag and Hg,[41] and led to the formation of a Ag/Hg amalgam. As a result, Tween 20 was displaced from the AgNPs surface. This can be seen in Fig. S4.† The gas chromatography analysis in Fig. S4† shows Tween 20 (often analysed with oxirane and 1,4-dioxane according to European Pharmacopoeia 6.0) in a dialysis solution with 100 nM Hg^{2+} (b) was higher than that without Hg^{2+} (c). This phenomenon clearly demonstrated the displacement of Tween 20 after the addition of Hg^{2+}. The removal of the stabilizer (Tween 20) caused the AgNPs to aggregate in high ionic strength solutions, which results in a sharp decrease of the absorbance of the AgNPs (Fig. 1 and S5†).

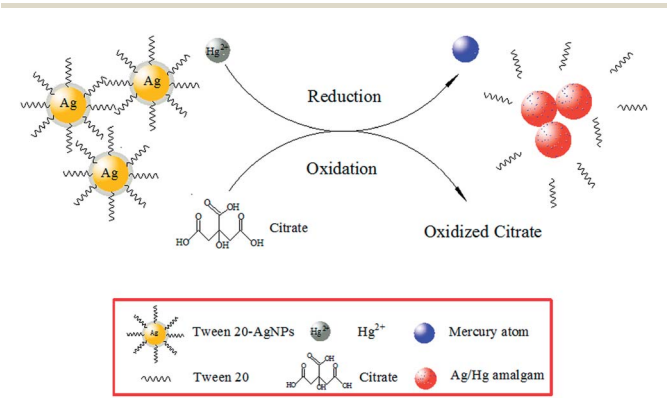

Fig. 1 Illustration of the mechanism of Tween 20-AgNPs sensing and co-stabilizing with Hg^{2+}.

To demonstrate the feasibility of our design, two control experiments were carried out: (1) to investigate whether Tween 20 has an effect on the sensor, a series of Hg^{2+} concentrations (0, 0.05, 0.2, 0.5, 5.0, 20.0, 50.0, 80.0, 100.0, 120.0, 140.0, 200.0, and 500.0 nM) were added to solutions of citrate-capped AgNPs. The UV-vis absorption decreased slightly with the addition of Hg^{2+} (Fig. 2A). The optimized linear fitting equation was $y = -0.00098x + 2.0726$ (where x is the concentration of Hg^{2+}, and y is the absorbance intensity), with the correlation coefficient of 0.50957 (Fig. 2B), which was far below the ideal value of 1.0. The result showed that the decrease in the absorbance intensity had little linear dependence on the concentration of Hg^{2+}, and the citrate-capped AgNPs were unstable in high ionic strength solutions. This assay demonstrated that AgNPs showed heterogeneous aggregation without a stabilizer and Tween 20 was essential in the availability of the sensor.

(2) To test the function of citrate ions in the detection of Hg^{2+}, citrate-capped AgNPs were replaced with bare AgNPs (without citrate ions capped on the surface) in the synthesis of Tween 20-AgNPs. Hg^{2+} (0, 100.0, 120.0, 140.0, and 200.0 nM) was employed as a model to confirm this effect (Fig. 3). The absorption showed little change when Hg^{2+} was added to the AgNPs solutions. In the absence of citrate ions, no significant reduction of Hg^{2+} occurred. This result indicated that citrate ions acted as a reducing agent for Hg^{2+}. To further demonstrate the reduction of Hg^{2+} with citrate ions, 35 μL of $Hg(NO_3)_2$ solutions of various concentrations were added to 3 mL 1.0 M citrate ions solution at room temperature to achieve the final Hg^{2+} concentrations of 0, 5.0, and 10.0 μM (we chose the higher concentration of Hg^{2+} for the better visual observation of the reduction. Citrate ions were prepared in 100 mM sodium phosphate solution with sodium citrate to achieve the final concentration of 1.0 mM.). The reduction solution was photographed and the residual Hg^{2+} concentration of the solution was determined by AFS after appropriate filtration and dilution. As shown in Fig. S6,† the addition of citrate ions induces obvious Hg^{2+} reduction and precipitation. AFS almost couldn't detect the residual Hg^{2+} after filtration and dilution. At the same time, the reducing ability could be seen from the standard electrode potentials: $E^0(Hg^{2+}/Hg) = 0.852$ V.[50] The electrode potential of citrate ions is −0.121 V in sodium phosphate buffer. So, citrate would reduce Hg^{2+} to elemental mercury in the sensor system. The results of the two control experiments indicated that Tween 20 played an important role in the probe in our present work, citrate ions acted as a reducing agent in the sensing process, and Hg^{2+} made a negligible contribution toward decreasing the absorbance of AgNPs.

3.2. Evidence for the formation of a Ag/Hg amalgam

To test the hypothesis mentioned above, we measured the absorbance spectra of Tween 20-AgNPs in the absence and presence of Hg^{2+} at 100, 120, 140, and 200 nM. The surface plasmon resonance wavelength of Tween 20-AgNPs appears at 400 nm (Fig. 4, curve a), and the resonance intensity showed little decrease compared to the citrate-capped AgNPs in the absence of Hg^{2+}, indicating that the AgNPs were well dispersed

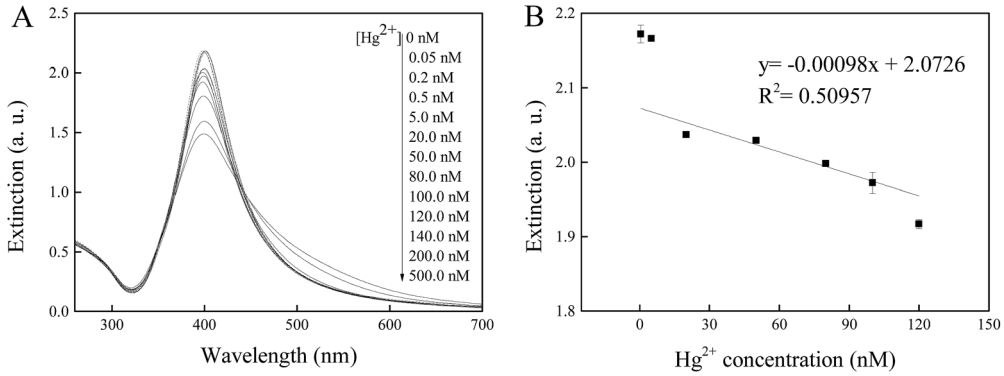

Fig. 2 (A) Extinction spectra of the working solutions containing citrate-capped AgNPs after adding various concentrations of Hg^{2+} (0–500.0 nM) in buffer. (B) Linear fitting line between the absorbance intensity and Hg^{2+} concentration in buffer. The concentrations of Hg^{2+} were 20.0, 50.0, 80.0, 100.0, and 120.0 nM. Every data point is the mean of three measurements. The error bars are the standard deviation.

in the phosphate solution. In other words, Tween 20 molecules could effectively protect citrate-capped AgNPs against aggregation in high ionic strength solutions. This phenomenon was consistent with the results of TEM characterization (Fig. S1C†). The Tween 20-AgNPs were shown to be uniform and monodisperse with a size distribution of 12.0–15.0 nm and an average size of 13.0 nm. EDX spectroscopy analysis showed the existence of Ag, without Hg (Fig. S7A and Table S1†). After adding 100 nM (Fig. 4, curve b), 120 nM (Fig. 4, curve c), 140 nM (Fig. 4, curve d) and 200 nM (Fig. 4, curve e) of Hg^{2+}, a decrease in the strength of the surface plasmon resonance band at ~400 nm and the formation of a new absorbance band at ~600 nm was observed, indicating the aggregation of Tween 20-AgNPs. The plasmon absorption band of the aggregates showed a small red shift with the increasing concentration of Hg^{2+}, while the area of this plasmon absorption band became greater relative to the plasmon absorption band of the citrate-capped AgNPs. TEM images (Fig. S1D†) revealed that the presence of Hg^{2+} led to the formation of an irregular Ag/Hg amalgam with a large size distribution of 20.0–30.0 nm. The structural composition of the Ag/Hg amalgam estimated from EDX spectra revealed the coexistence of Ag and Hg elements (Fig. S7B and Table S2†). The XRD analysis in Fig. S8† further demonstrates that the Ag/Hg amalgam was a mixture of Ag_2Hg_3 and $Ag_{1.1}Hg_9$ complexes. The high Hg^{2+} concentration led to an increase of the $Ag_{1.1}Hg_9$ complex and a relative decrease of Ag_2Hg_3, which could be seen from the change of diffraction peak.

To further demonstrate the formation of a Ag/Hg amalgam, evidence that was more visually intuitive is shown in Fig. S9.† Fig. S9† shows that the yellow solution of AgNPs turned red brown with the addition of 100 nM Hg^{2+} and further turned drab olive with 200 nM Hg^{2+} due to increased Ag/Hg amalgam precipitation.

3.3. Optimization of the amalgamation and aggregation conditions

In this study, the amalgamation and aggregation time and reacting temperature are crucial for the probe sensitivity. Although longer amalgamation and aggregation time may yield

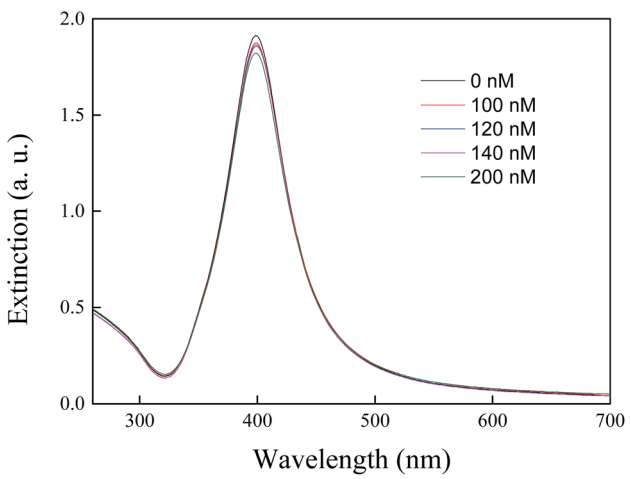

Fig. 3 Extinction spectra of the working solutions containing Tween 20-modified bare AgNPs after adding 0, 100.0, 120.0, 140.0 and 200.0 nM Hg^{2+} in buffer.

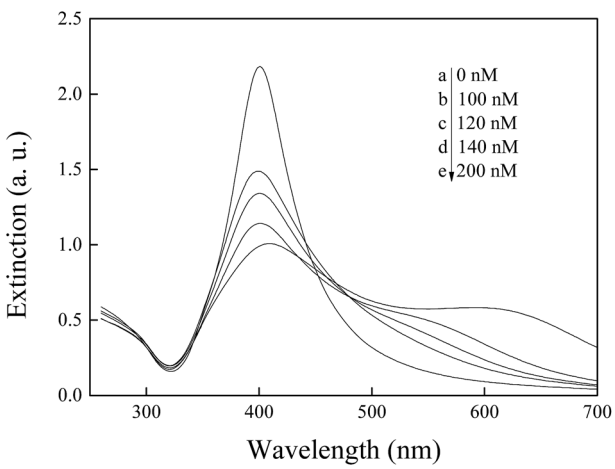

Fig. 4 Extinction spectra of working solutions containing Tween 20-AgNPs after adding 0, 100.0, 120.0, 140.0, 200.0 nM Hg^{2+} in buffer.

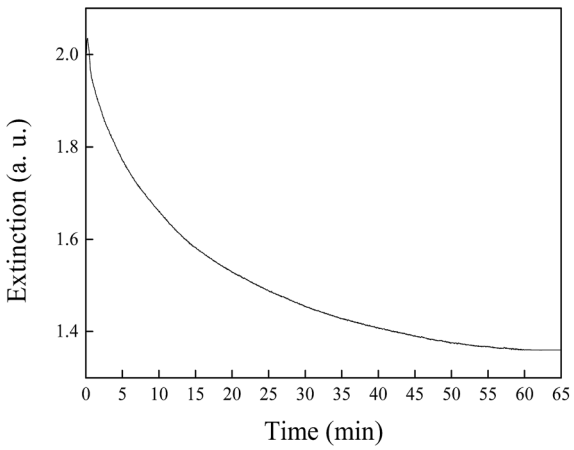

Fig. 5 Optimizing experiment of the amalgamation and aggregation time. A value of 100 nM was selected as the Hg^{2+} concentration to determine the optimum amalgamation and aggregation time. The UV-vis absorption value was recorded at 400 nm.

a more stable absorbance signal, it is unnecessary if the system has reached equilibrium. To obtain the optimal reaction time, the kinetics of amalgamation and aggregation were measured. Fig. 5 shows the UV-vis absorbance intensity reaction time curve for the addition of 100 nM Hg^{2+} to a solution of AgNPs. The UV-vis absorbance was found to decrease with the increase in amalgamation and aggregation time, then reached a minimum at 58 min, and was nearly constant until 65 min. Based on these observations, we chose 60 min as the optimum reaction time to ensure completeness of amalgamation and aggregation. To facilitate Hg^{2+} detection, indoor temperature (25–27 °C) was chosen as the operational temperature for all experiments. All the experiments were conducted using these optimized conditions.

3.4. DLS probing the agglomeration process

To investigate the process of amalgamation and aggregation, the size distribution was measured with DLS at various times (0, 10, 20, 30, 40, 50, 60, 70 and 80 min) after addition of 100 nM Hg^{2+}. As shown in Fig. 6, the average initial size of 30.3 nm (the different size compared to the TEM results was because of the two different measurement principles) of the Tween 20-AgNPs increased tremendously to 176.9 nm within 10 min and further reached 203.0 nm within 20 min. After 30 min, the size increased a little slower, with the size reaching 209.0 nm. After this, the average size showed nearly no change with time. This trend was consistent with the curve in Fig. 5, indicating that the amalgamation and aggregation process mainly occurred within the first 20 min and was almost completed within 60 min.

3.5. Sensitivity for Hg^{2+}

Based on the above proposed strategy and optimized assay conditions, various concentrations of Hg^{2+} were added to the buffer to evaluate the sensitivity of the Tween 20-AgNPs probe for Hg^{2+} detection. The various concentrations of Hg^{2+} were 0, 0.05, 0.2, 0.5, 5.0, 20.0, 50.0, 80.0, 100.0, 120.0, 140.0, 200.0, and 500.0 nM. As shown in Fig. 7A, higher concentrations of Hg^{2+} resulted in a gradual decrease of the UV-vis absorbance. It was

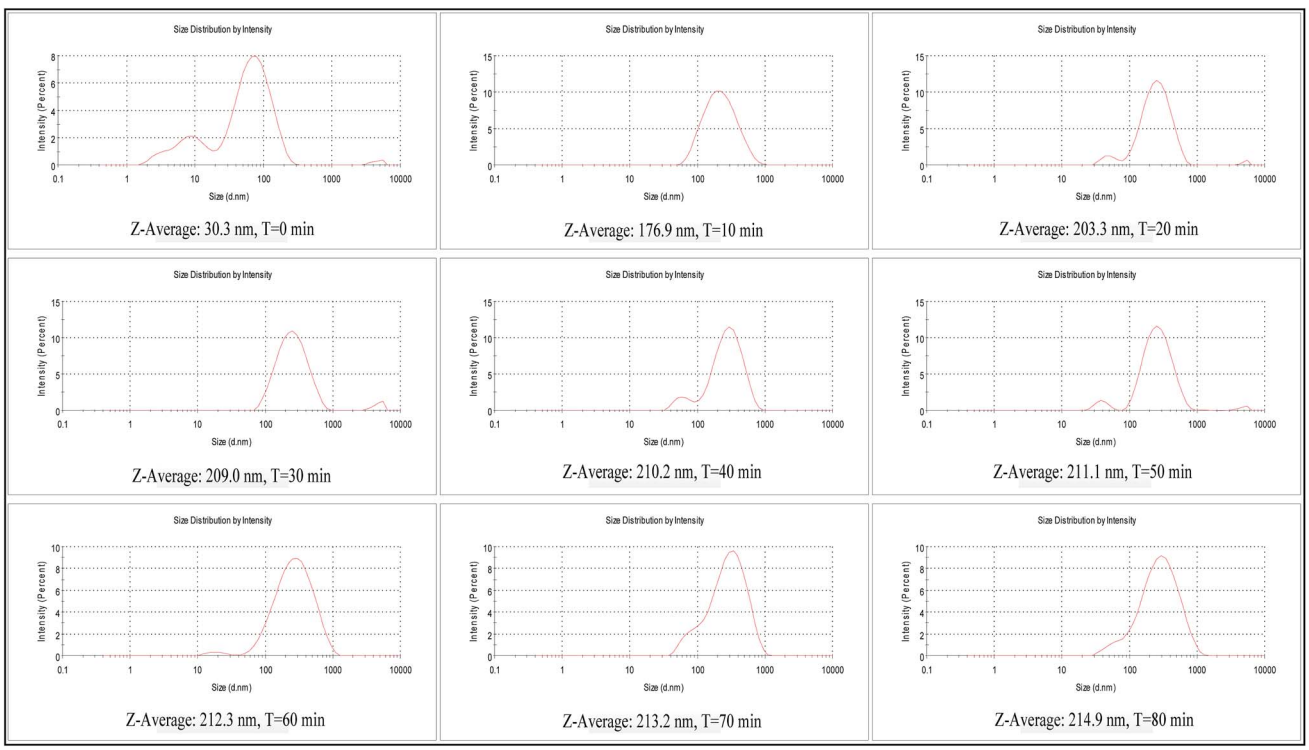

Fig. 6 DLS probing the agglomeration process.

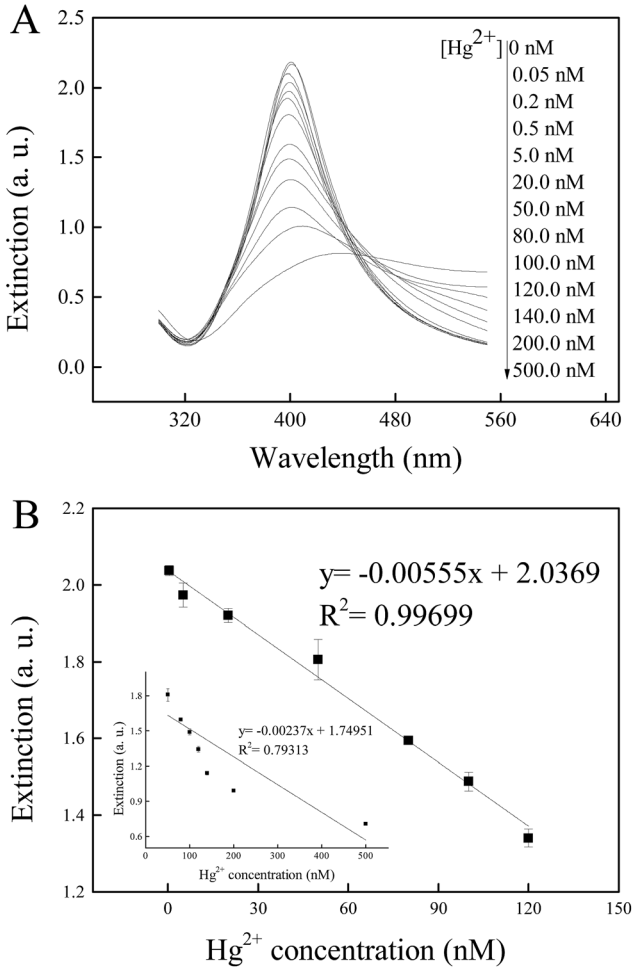

Fig. 7 (A) Extinction spectra of the working solutions containing Tween 20-AgNPs after adding various concentrations of Hg^{2+} (0–500.0 nM) in buffer. (B) Linear relationship between the absorbance intensity and Hg^{2+} concentration in buffer. The concentrations of Hg^{2+} are 0.5, 5.0, 20.0, 50.0, 80.0, 100.0, and 120.0 nM in (B) and 50.0, 80.0, 100.0, 120.0, 140.0, 200.0, 500.0 nM in the inset. Every data point is the mean of three measurements. The error bars are the standard deviation.

obvious that, even at very low Hg^{2+} concentrations (0.05 nM), the absorbance intensity exhibited a distinct change, which indicated that the proposed probe was sensitive enough for Hg^{2+} detection.

Fig. 7B shows the linear relationship between the decrease in the UV-vis absorbance intensity and Hg^{2+} concentration. The absorbance intensity was found to show a linear dependence on the concentration of Hg^{2+} in the range of 0.5–120 nM (the citrate ions of Tween 20-AgNPs was demonstrated to be sufficient to reduce Hg^{2+} as showing later in Fig. 10). The linear relationship was described by the equation of $y = -0.00555x + 2.0369$ (where x is the concentration of Hg^{2+}, and y is the absorbance intensity), with a correlation coefficient of 0.99699. However, the correlation coefficient decreased when the highest Hg^{2+} concentration studied (500.0 nM) was taken into account ($r^2 = 0.79313$, inset in Fig. 7B). The limit of detection (LOD) was estimated to be 0.31 nM, as calculated with the following equation: LOD = $3\sigma/\kappa$, where κ is the slope of the calibration curve, and σ is the standard deviation for 10 measurements of the blank solution. This LOD was low enough to meet the need for trace Hg^{2+} detection when compared with previously reported methods (Table S3†). Moreover, the LOD was sufficient for the detection of Hg^{2+} in drinking water, and was far below the mandated limit of 2.0 ppb set by the U.S. Environmental Protection Agency (EPA).[51] The wide dynamic range undoubtedly improves the applications of this probe.

Fig. S10† shows the concentration dependent colorimetric response of the assay. In the Hg^{2+} concentration range of 0.5–200.0 nM, the absorbance intensity decreased regularly. The response of the assay is linear, with a linear regression correlation coefficient of 0.98104 for this wider Hg^{2+} concentration range of 0.5–200.0 nM (inset in Fig. S10†).

3.6. Selectivity of the probe

To study the selectivity of this probe, the UV-vis absorption responses of the Tween 20-AgNPs method to Hg^{2+} and other metal ions, including K^+, Ca^{2+}, Mg^{2+}, Li^{2+}, Pb^{2+}, Zn^{2+}, Mn^{2+}, Ni^{2+}, Cr^{3+}, Fe^{3+}, Co^{2+}, Cu^{2+}, Cd^{2+}, and Al^{3+}, were assayed using the optimized conditions. In addition, selectivity experiments were performed for a mixture of all the metal ions with and without Hg^{2+}. The concentrations of Hg^{2+} and the other metal ions were 100 nM and 1 μM, respectively. In contrast with the significantly greater absorption decrease observed for Hg^{2+}, far weaker changes were observed upon the addition of μM concentrations of the other tested metal ions (Fig. 8), revealing that this probe is selective for Hg^{2+}.

However, Cu^{2+} resulted in a slight increase in the colorimetric assay response. The magnitude of the response to Cu^{2+} was considerably smaller than the response of the assay to Hg^{2+}, even though the concentration of Cu^{2+} was 10-fold higher than the concentration of Hg^{2+}. Additionally, although the addition of the mixed metal ions without Hg^{2+} resulted in a slightly higher absorption intensity decrease than that observed for the

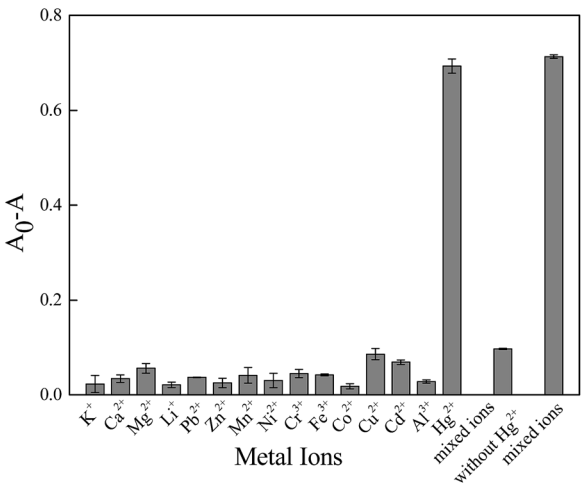

Fig. 8 UV-vis absorption extinction value in the presence of various metal ions. The concentration is 1 μM for each metal ion and 100 nM for Hg^{2+}. The UV-vis absorption value was recorded at 400 nm.

individual metal ions, the decrease was far greater in the presence of Hg^{2+}. These results indicated that the probe is not only insensitive to the other metal ions, but also selective toward Hg^{2+} when they are present. This method has a strong anti-interference capability and excellent selectivity to detect trace Hg^{2+} in environmental and biological fields.

3.7. Effect of surfactant chain length

To explore the effect of surfactant chain length on the absorption change of the AgNPs, Tween 20 was replaced with Tween 40, Tween 60, and Tween 80. As shown in Fig. 9, a small absorption decrease was observed on addition of Hg^{2+} to Tween 40-modified AgNPs. Similar phenomena were observed for Tween 60- and Tween 80-modified AgNPs. These results indicated that Tween 20 played a crucial role in the feasibility of the probe for Hg^{2+} detection.

3.8. Co-stability of Hg^{2+}

In this study, Hg^{2+} was reduced to Hg^0, which then formed a Ag/Hg amalgam with AgNPs. The Ag/Hg amalgam was not stable in the environment due to the removal of the Tween 20 stabilizer and aggregated from the solutions. To evaluate the co-stability efficiency, the Hg^{2+} and AgNPs concentrations were determined after filtration using our method and AAS. As shown in Fig. 10A, the AgNPs removal efficiency improved with the increase of Hg^{2+} concentration. The results showed no Hg^{2+} was detected in solution with our proposed method. Fig. 10B indicates that the AgNPs removal percentage (the amount of AgNPs removed from solution, calculated by mass concentration of silver) correlated well with the concentration of Hg^{2+} in the range 2×10^{-8} to 2×10^{-7} M. The linear relationship was described by the equation $y = 0.07538x$ (where x is the concentration of Hg^{2+}, and y is the AgNPs removal percentage) with a correlation coefficient of 0.99862.

Fig. S11† exhibits a more intuitive demonstration of the co-stability efficiency. After standing for five hours, the solutions were filtered. As shown in Fig. S11,† the yellow filtrate (the color mainly caused by Tween 20-AgNPs) turned red (the color of the Ag/Hg amalgam), and then colorless with the increase of Hg^{2+} concentration. These results indicated that higher Hg^{2+} concentrations resulted in better AgNPs removal efficiency.

In order to evaluate the AgNPs removal efficiency when the concentration of Hg^{2+} was in excess, Tween 20-AgNPs (0.5, 1.0, 2.0, 8.0, 10.0, 12.0, 15.0, and 17.0 μg mL^{-1}) were added to a solution containing 500 nM Hg^{2+}. As shown in Fig. 11, the AgNPs removal efficiency increased with the concentration of Tween 20-AgNPs because more Ag/Hg amalgam is generated in the solutions with more Tween 20-AgNPs. The linear relationship between the AgNPs removal percentage and the concentration of Tween 20-AgNPs (inset of Fig. 11) was described by the linear fitting line $y = 3.17038x$ (where x is the concentration of Tween 20-AgNPs, and y is the AgNPs removal percentage) with a correlation coefficient of 0.994.

3.9. Assay for Hg^{2+} concentration in water samples

Because our method showed excellent selectivity and sensitivity in buffer solutions, this method was employed for Hg^{2+}

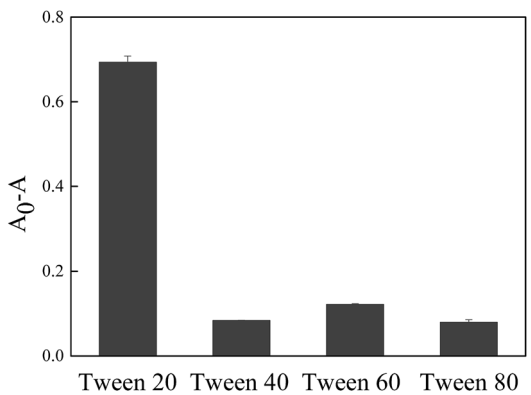

Fig. 9 UV-vis absorption extinction value of Tween 20- 40-, 60-, and 80-modified AgNPs after adding 100 nM Hg^{2+}. The UV-vis absorption value was recorded at 400 nm.

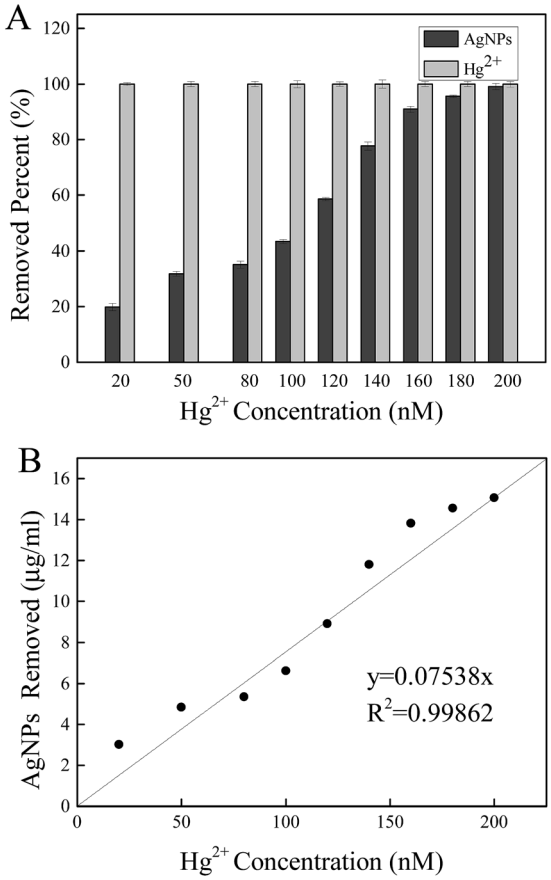

Fig. 10 (A) Co-stability of AgNPs with Hg^{2+} in a solution containing 15.204 μg mL^{-1} Tween 20-AgNPs after adding 20.0, 50.0, 80.0, 100.0, 120.0, 140.0, 160.0, 180.0, and 200.0 nM Hg^{2+} in buffer. (B) Linear relationship between the AgNPs removal percentage and Hg^{2+} concentration in buffer. Every data point is the mean of three measurements. The error bars are the standard deviation. The UV-vis absorption value was recorded at 400 nm.

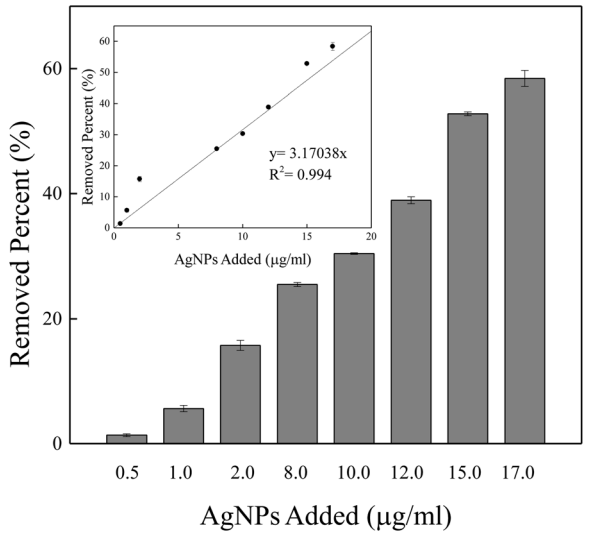

Fig. 11 Co-stability of AgNPs with Hg^{2+} in a solution containing 500 nM Hg^{2+} after adding 0.5, 1.0, 2.0, 8.0, 10.0, 12.0, 15.0, and 17.0 μg mL^{-1} Tween 20-AgNPs in buffer. Inset is the linear relationship between the AgNPs removal percentage and the amount of Tween 20-AgNPs added in buffer. Every data point is the mean of three measurements. The error bars are the standard deviation. The UV-vis absorption value was recorded at 400 nm.

detection in several environmental water samples to evaluate its practical application. Tap water, spring water, and surface water samples, spiked with 0, 20, 50, and 100 nM Hg^{2+}, were chosen for the study. For tap water experiments, the sample was collected after discharging tap water for ~15 min and boiling for 5 min to remove chlorine. For spring water and surface water experiments, the samples collected were first filtered by qualitative filter paper and then centrifuged for 15 min at 10 000 rpm to remove oils and microbe impurities. The background concentration of mercury in the water samples was measured to be less than 0.1 nM by AFS. All the Hg^{2+}-spiked water samples were analyzed using our Tween 20-AgNPs method according to the general procedure with five replicates and compared with the AFS results. The results are summarized in Table S4† and showed good agreement with the expected values and the values determined by AFS. The results revealed high consistency in the determination of Hg^{2+} concentrations in environmental water samples by the proposed Tween 20-AgNPs method and using conventional instrumentation, demonstrating the excellent performance of this probe in practical applications.

4. Conclusions

In summary, a rapid and sensitive colorimetric sensing strategy for Hg^{2+} detection is presented. Hg^{2+} induced the amalgamation and aggregation of Tween 20-AgNPs and therefore, was quantified by the subsequent UV-vis changes. This strategy showed high selectivity and sensitivity to Hg^{2+}. Moreover, the probe exhibited excellent co-stability properties with Hg^{2+} and was successfully applied in the detection of Hg^{2+} in water samples.

Acknowledgements

This study was financially supported by the National Natural Science Foundation of China (51178171, 51039001, 41271294).

Notes and references

1 T. A. Baughman, *Environ. Health Perspect.*, 2006, **114**, 147–152.
2 I. Hoyle and R. D. Handy, *Aquat. Toxicol.*, 2005, **72**, 147–159.
3 L. Campbell, D. G. Dixon and R. E. Hecky, *J. Toxicol. Environ. Health, Part B*, 2003, **6**, 325–356.
4 C. M. Wood, M. D. McDonald, P. Walker, M. Grosell, J. F. Barimo, R. C. Playle and P. J. Walsh, *Aquat. Toxicol.*, 2004, **70**, 137–157.
5 D. P. Wojcik, M. E. Godfrey, D. Christie and B. E. Haley, *Neuroendocrinol. Lett.*, 2006, **27**, 415–423.
6 J. W. Sekowski, L. H. Malkas, Y. Wei and R. J. Hickey, *Toxicol. Appl. Pharmacol.*, 1997, **145**, 268–276.
7 J. L. Barriada, A. D. Tappin, E. H. Evans and E. P. Achterberg, *TrAC, Trends Anal. Chem.*, 2007, **26**, 809–817.
8 H. Erxleben and J. Ruzicka, *Anal. Chem.*, 2005, **77**, 5124–5128.
9 S. Gil, I. Lavilla and C. Bendicho, *Anal. Chem.*, 2006, **78**, 6260–6264.
10 Y. F. Li, C. Y. Chen, B. Li, J. Sun, J. X. Wang, Y. X. Gao, Y. L. Zhao and Z. F. Chai, *J. Anal. At. Spectrom.*, 2006, **21**, 94–96.
11 B. M. W. Fong, T. S. Siu, J. S. K. Lee and S. Tam, *J. Anal. Toxicol.*, 2007, **31**, 281–287.
12 S. J. Lee and M. Moskovits, *Nano Lett.*, 2011, **11**, 145–150.
13 Y. X. Du, R. Y. Liu, B. H. Liu, S. H. Wang, M. Y. Han and Z. P. Zhang, *Anal. Chem.*, 2013, **85**, 3160–3165.
14 A. H. Miguel and C. M. Jankowski, *Anal. Chem.*, 1974, **46**, 1832–1834.
15 Y. Bonfil, M. Brand and E. Kirowa-Eisner, *Anal. Chim. Acta*, 2000, **424**, 65–76.
16 H. J. Kim, D. S. Park, M. H. Hyun and Y. B. Shim, *Electroanalysis*, 1998, **10**, 303–306.
17 R. Mikelova, J. Baloun, J. Petrlova, V. Adam, L. Havel, J. Petrek, A. Horna and R. Kizek, *Bioelectrochemistry*, 2007, **70**, 508–518.
18 A. Ono and H. Togashi, *Angew. Chem., Int. Ed.*, 2004, **43**, 4300–4302.
19 A. Coskun and E. U. Akkaya, *J. Am. Chem. Soc.*, 2006, **128**, 14474–14475.
20 S. K. Ko, Y. K. Yang, J. Tae and I. Shin, *J. Am. Chem. Soc.*, 2006, **128**, 14150–14155.
21 A. Swarnkar, G. S. Shanker and A. Nag, *Chem. Commun.*, 2014, **50**, 4743–4746.
22 A. Ajayaghosh, *Acc. Chem. Res.*, 2005, **38**, 449–459.
23 S. Pattanayak, A. Swarnkar, A. Priyam and G. M. Bhalerao, *Dalton Trans.*, 2014, 11826–11833.
24 Y. K. Yang, K. J. Yook and J. Tae, *J. Am. Chem. Soc.*, 2005, **127**, 16760–16761.

25 S. Yoon, A. E. Albers, A. P. Wong and C. J. Chang, *J. Am. Chem. Soc.*, 2005, **127**, 16030–16031.
26 J. B. Wang, X. H. Qian and J. N. Cui, *J. Org. Chem.*, 2006, **71**, 4308–4311.
27 E. M. Nolan and S. J. Lippard, *J. Am. Chem. Soc.*, 2007, **129**, 5910–5918.
28 K. Bera, A. K. Das, M. Nag and S. Basak, *Anal. Chem.*, 2014, **86**, 2740–2746.
29 Y. Hu, L. J. Meng and Q. H. Lu, *Langmuir*, 2014, **30**, 4458–4464.
30 Z. Fang, K. Y. Pu and B. Liu, *Macromolecules*, 2008, **41**, 8380–8387.
31 J. W. Liu and Y. Lu, *Angew. Chem., Int. Ed.*, 2007, **46**, 7587–7590.
32 D. Li, A. Wieckowsk and I. Willner, *Angew. Chem., Int. Ed.*, 2008, **47**, 3927–3931.
33 M. Hollenstein, C. Hipolito, C. Lam, D. Dietrich and D. M. Perrin, *Angew. Chem.*, 2008, **47**, 4346–4350.
34 S. M. Jia, X. F. Liu, P. Li, D. M. Kong and H. X. Shen, *Biosens. Bioelectron.*, 2011, **27**, 148–152.
35 P. Chen and C. He, *J. Am. Chem. Soc.*, 2004, **126**, 728–729.
36 Z. Gu, M. X. Zhao, Y. W. Sheng, L. A. Bentolila and Y. Tang, *Anal. Chem.*, 2011, **83**, 2324–2329.
37 Y. Bhattacharjee and A. Chakraborty, *ACS Sustainable Chem. Eng.*, 2014, **2**, 2149–2154.
38 C. Y. Lin, C. J. Yu, Y. H. Lin and W. L. Tseng, *Anal. Chem.*, 2010, **82**, 6830–6837.
39 K. Y. Pu, Z. T. Luo, K. Li, J. P. Xie and B. Liu, *J. Phys. Chem. C*, 2011, **115**, 13069–13075.
40 M. Koneswaran and R. Narayanaswamy, *Sens. Actuators, B*, 2009, **139**, 91–96.
41 M. Li, Q. Y. Wang, X. D. Shi, L. A. Hornak and N. Q. Wu, *Anal. Chem.*, 2011, **83**, 7061–7065.
42 R. Freeman, T. Finder and I. Willner, *Angew. Chem., Int. Ed.*, 2009, **48**, 7818–7821.
43 T. J. O'Shea and S. M. Lunte, *Anal. Chem.*, 1993, **65**, 247–250.
44 F. Jelen, B. Yosypchuk, A. Kourilova, L. Novotny and E. Palecek, *Anal. Chem.*, 2002, **74**, 4788–4793.
45 P. Juskova, V. Ostatna, E. Palecek and F. Foret, *Anal. Chem.*, 2010, **82**, 2690–2695.
46 L. Deng, X. Y. Ouyang, J. Y. Jin, C. Ma, Y. Jiang, J. Zheng, J. S. Li, Y. H. Li, W. H. Tan and R. H. Yang, *Anal. Chem.*, 2013, **85**, 8594–8600.
47 Z. M. Xiu, J. Ma and P. J. J. A. lvarez, *Environ. Sci. Technol.*, 2011, **45**, 9003–9008.
48 J. Y. Liu and R. H. Hurt, *Environ. Sci. Technol.*, 2010, **44**, 2169–2175.
49 C. C. Huang and W. L. Tseng, *Analyst*, 2009, **134**, 1699–1705.
50 T. T. Lou, Z. P. Chen, Y. Q. Wang and L. X. Chen, *ACS Appl. Mater. Interfaces*, 2011, **3**, 1568–1573.
51 http://water.epa.gov/drink/contaminants/basicinformation/mercury.cfm#four.